# Semiconductor coupled solar photo-Fenton's treatment of dyes and textile effluent

Jeevitha R. Raji and Kandasamy Palanivelu[*]

*Centre for Environmental Studies, Anna University, Chennai 600 025, India*

**Abstract.** NanoTiO$_2$ was synthesized by ultrasonication assisted sol-gel process and subjected to iron doping and carbon-iron codoping. The synthesized catalysts were characterized by XRD, HR-SEM, EDX, UV-Vis absorption spectroscopy and BET specific surface area analysis. The average crystallite size of pure TiO$_2$ was in the range of 30 - 33 nm, and that of Fe-TiO$_2$ and C-Fe TiO$_2$ was in the range of 7 - 13 nm respectively. The specific surface area of the iron doped and carbon-iron codoped nanoparticles was around 105 m$^2$/g and 91 m$^2$/g respectively. The coupled semiconductor photo-Fenton's activity of the synthesized catalysts was evaluated by the degradation of a cationic dye (C.I. Basic blue 9) and an anionic dye (C.I. Acid orange 52) with concurrent investigation on the operating variables such as pH, catalyst dosage, oxidant concentration and initial pollutant concentration. The most efficient C-Fe codoped catalyst was found to effectively destruct synthetic dyes and potentially treat real textile effluent achieving 93.4% of COD removal under minimal solar intensity (35-40 kiloLUX). This reveals the practical applicability of the process for the treatment of real wastewater in both high and low insolation regimes.

**Keywords:** TiO$_2$ nanoparticles; carbon-iron codoping; dyes; textile effluent; solar photocatalysis; low insolation

## 1. Introduction

Textile industries have been the foremost contributor towards world's economy in the past decades. But in the recent years, textile industries are also recognized as a major source of pollution, as the untreated dyes released into the textile effluent form potentially carcinogenic amines putting forward a serious threat to the environment (Lucas and Peres 2006, Konecoglu *et al*. 2015). The limitations associated with the conventional treatment technologies viz., toxicity in chlorination; high energy and capital cost in ozonation, electrochemical oxidation and sonication impair their application in the effective treatment of textile wastewater. Hence, there is a necessity to develop a cleaner, greener and cost-effective technology for the destruction of dye pollutants. In this sense, TiO$_2$ photocatalysis has attracted a great deal of attention in destructing variety of dyes, and titania nanoparticles have received a chief-most primacy due to the large fraction of surface atoms (Avisar *et al*. 2001, Kamat and Dan 2002).

On the other hand, in lieu of the superior efficiency, the drawback associated with TiO$_2$

---

*Corresponding author, Professor, E-mail: kpvelu@annauniv.edu
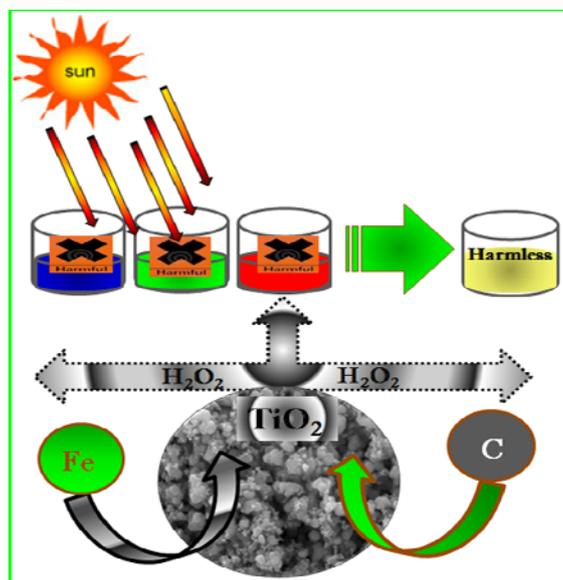
Graphical representation of the current study

photocatalylsis is that the photoreactions on the most active form of $TiO_2$ could only be induced by ultraviolet (UV) light sources, intensifying the current energy demand. One of the possible solutions to this energy challenge with simultaneous destruction of dye pollutants is to make efficient use of natural solar energy by a robust technology. Metal/non-metal doping is one such technology which is believed to enhance the photoactivity of $TiO_2$ under natural sunlight (Murray *et al*. 2000). Codoped titania with metal-nonmetal elements has attracted more attention since the detrimental recombination effect associated with monodoping could be passivated by co-doping (Li *et al*. 2010, Hussain and Siddiqa 2011, Kavitha *et al*. 2013). Very recently, heterogeneous Fenton's system coupled with doped/codopedTiO$_2$ photocatalysis is also identified to remarkably degrade refractory dye pollutants without generating sludge as witnessed in conventional homogeneous Fenton's treatment systems (Oliveria *et al*. 2007, Navalon *et al*. 2010, Zhao *et al.* 2010, Hamadanian *et al.* 2011).

In our earlier works, carbon doped titania nanoparticles (Jeevitha Raji and Palanivelu 2011) and iron doped titania fibers (Jeevitha Raji *et al*. 2013) were prepared and their photocatalytic performance was evaluated. The present work is emphasized on i) doping and co-doping of pristine $TiO_2$ nanoparticles with iron and carbon-iron  ii) evaluation of the semiconductor coupled photo-Fenton's activity of doped and codoped titania in the degradation of basic blue 9 (BB) and acid orange 52 (AO) under natural sunlight iii) Applying the optimized conditions in the treatment of real textile effluent.

## 2. Materials and methods

### 2.1 Materials

All chemicals used in the present study were of analytical grade. Titanium (IV) propoxide (Sigma Aldrich), isopropyl alcohol (Samchun Chemical), coconut oil (Parachute Pure), ferrous sulphate heptahydrate (Samchun Chemical), basic blue 9 (Merck) and acid orange 52 (Merck) were used as received from the suppliers without further purification. All reagents and solutions were prepared using double distilled water.

### 2.2 Synthesis of pristine, iron doped and carbon-iron codoped TiO$_2$ nanoparticles

Pristine TiO$_2$ was prepared by ultrasonication assisted sol-gel process with titanium isopropoxide as the titania precursor and designated as Pure-TiO$_2$NP (Jeevitha Raji and Palanivelu 2011). Pure-TiO$_2$NP was subjected to iron doping by wet impregnation method in a series of ferrous sulphate solutions containing 0.2 wt%, 0.5 wt%, 1.0 wt%, and 2.0 wt% of Fe$^{2+}$ ion. The resulting iron doped catalysts were then designated as, "Fe$_{0.2}$TiO$_2$NP, Fe$_{0.5}$TiO$_2$NP, Fe$_{1.0}$TiO$_2$NP and Fe$_{2.0}$TiO$_2$NP" respectively.

In the C-Fe co-doping process, Pure-TiO$_2$NP was first subjected to carbon doping process with coconut oil as carbon precursor (Jeevitha Raji and Palanivelu 2011), where the coconut oil to titania ratio was varied as 2.0 wt% and 4.0 wt%. It was then subjected to co-doping with iron by wet impregnation method, in which the proportion of iron was varied as 1.0 wt% and 2.0 wt%. The resulting carbon-iron codoped catalysts were designated as C$_{2.0}$Fe$_{1.0}$TiO$_2$NP, C$_{2.0}$Fe$_{2.0}$TiO$_2$NP, C$_{4.0}$Fe$_{1.0}$TiO$_2$NP and C$_{4.0}$Fe$_{2.0}$TiO$_2$NP respectively.

### 2.3 Catalyst characterization

The crystal phase and crystalline nature of the catalysts were determined by powder X-ray diffraction patterns. ET 816 X-ray diffractometer was used to obtain high angle Powder X-ray diffraction patterns ($2\theta$=10.000 to 70.000) using Cu K$\alpha$ radiation ($\lambda$=1.5405 Å) with scintillation counter as detector. The surface morphology of the synthesized catalysts was characterized by High Resolution Scanning Electron Microscope using Hitachi S-3400 N with gold coating. In order to estimate the quantity of iron doped in TiO$_2$, EDX analysis was performed using Energy Dispersive X-ray spectrometer (Hitachi S-3400 N). The visible light absorption characteristics of the catalysts were investigated by UV-Vis spectrophotomer (Cary 5E). The specific surface area was determined by BET surface area analysis (Micrometrics ASAP2020) with N$_2$ physisorption.

### 2.4 Coupled semiconductor photo-Fenton's experiments

The photochemical experiments were carried out in 600 mL capacity glass cylindrical cells with 200 mL of working solution containing 0.1 g of catalyst and 10 ppm of BB/AO dye. The diameter and length of the glass reactor was 10 cm and 12.5 cm respectively; and the length of the reactant suspension was 3.5 cm respectively. The pH adjustments of the dye solutions were carried out by the addition of diluted NaOH/H$_2$SO$_4$ and all the reactant suspensions were first subjected to dark adsorption for 30 min to attain the adsorption equilibrium. After adsorption, hydrogen peroxide (29.7 mmol/L) was added and the reactant suspensions were immediately subjected to daylight solar irradiation between 10:00 A.M. to 2:00 P.M., when the intensity of sunlight was between 90 kilo LUX and 35 kilo LUX, measured using LUX meter (Model: TES 1332).

Textile wastewater (exhausted dye bath effluent) was collected from a small scale fabric dyeing industry located at Erode district of Tamil Nadu, India. The major dyes used for the fabric dyeing

were Yellow 186, Red 23 and Blue 21. The collected wastewater was screened to remove floatable solids, sand filtered to remove suspended solids and subjected to semiconductor coupled photo-Fenton's process.

During adsorption and irradiation, the dye decolorization was studied by collecting the aliquots, centrifuging and measuring the absorbance of supernatant at the $\lambda$ max of the dye (BB dye: 668 nm from pH 3 to pH 9; AO dye: 506 nm below pH 4 and 468 nm from pH 4 to pH 9) using a spectrophotometer (Model: Systronics Visiscan 167). Degradation of dyes was determined by Chemical Oxygen Demand (COD) following open reflux dichromate titrimetric method as described in Standard Methods (APHA 2005). Mineralization studies were accomplished by analysing Total Organic Carbon (TOC) using TOC analyser (Analytikjena, Germany multi N/C 2100S).
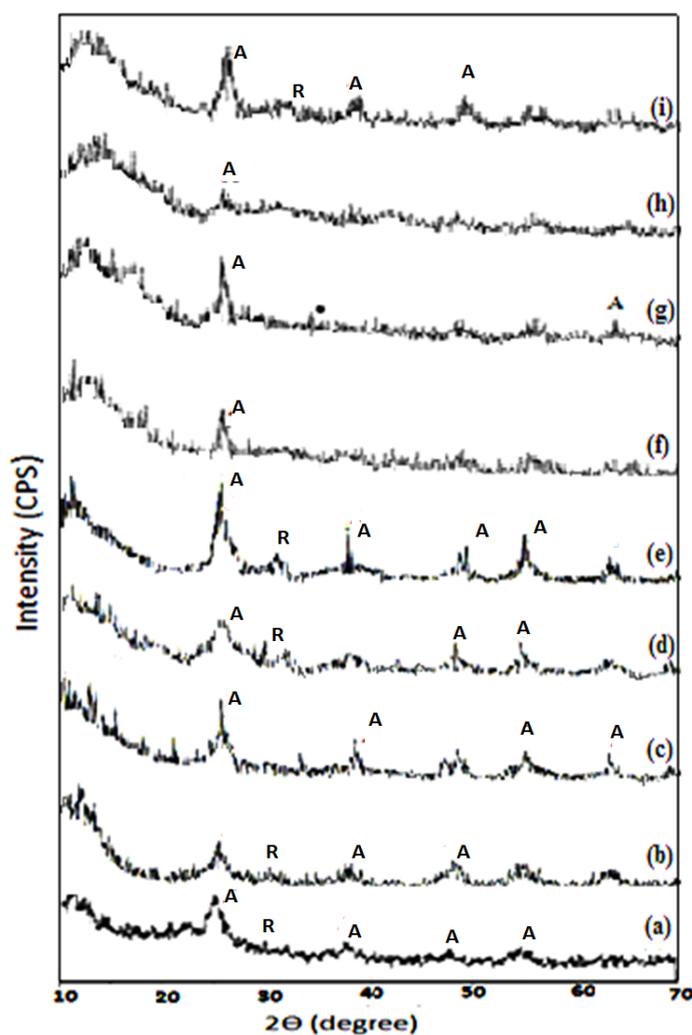


Fig. 1 X-ray diffraction patterns of (a) Pure $TiO_2$ NP (b) $Fe_{0.2}TiO_2NP$ (c) $Fe_{0.5}TiO_2NP$ (d) $Fe_{1.0}TiO_2NP$ (e) $Fe_{2.0}TiO_2NP$ (f) $C_{2.0}Fe_{1.0}TiO_2NP$ (g)$C_{2.0}Fe_{2.0}TiO_2NP$ (h) $C_{4.0}Fe_{1.0}TiO_2NP$ (i) $C_{4.0}Fe_{2.0}TiO_2NP$

## 3. Results and discussion

### 3.1 Crystal characterization

Powder X-ray diffraction patterns of the pristine, iron doped and carbon-iron codoped $TiO_2$ catalysts are presented in Fig. 1. For all the catalysts, the peaks corresponding to anatase phase were entirely observed at the $2\theta$ values of 25°, 37°, 48°, 55° and 62° revealing the predominant presence of anatase phase (Korosi *et al.* 2007), which might be attributed to the low temperature calcination of $TiO_2$ (at 145°C to 150°C). Using Scherrer's formula (Eq. (1)), the average particle size of the catalysts was calculated accounting the FWHM of high intense anatase peak (Zhao *et al.* 2010, Jongsomjit *et al.* 2005, McEvoy *et al.* 2013)

$$D_{Scherrer} = \frac{k\lambda}{\beta \cos\theta} \tag{1}$$

where,
    K=0.9 a shape factor for spherical particles
    $\lambda$=the wavelength of the incident radiation ($\lambda$=0.154 nm)
    $\theta$=half of the diffraction angle (deg)
    $\beta$=B - b the line broadening (rad). B is the full width at half maximum (FWHM) of the measured diffraction peak and b is the instrumental broadening
    The average crystallite size of pure titania was found to be in the range of 30-33 nm and that of Fe-$TiO_2$ nanoparticles was in the range of 7-12 nm showing a significant influence on the particle size of pure $TiO_2$ after iron doping. The average particle size of C-Fe nanoparticles was found to be in the range of 7-13 nm which was similar to that of Fe-$TiO_2$ nanopartilces.
    From Spurr formula (Eq. (2)), the sample '$C_{2.0}Fe_{2.0}TiO_2NP$' was found to be composed of a suitable fraction of 66% anatase and 34% rutile phases respectively

$$X_R = \frac{1}{1 + 0.8 \ (I_A / I_R)} \tag{2}$$

where, $I_A$ and $I_R$=Integrated peak intensities of anatase and rutile peaks respectively.

### 3.2 Morphological characterization

The SEM micrographs of the pure, doped and codoped catalysts are shown in Fig. 2
    From the SEM micrographs, all the iron doped titania catalysts were found to exist as distinct particles and the degree of agglomeration decreased as the amount of iron increased.
    It could be noticed that unlike in the SEM micrographs of pure and iron doped catalysts, the micrographs of the codoped catalysts were found to contain fine dispersed particles on the surface with increase in the amount of iron, which may represent the particles of iron oxide.

### 3.3 Compositional analysis

To estimate the amount of iron accounting for photo-Fenton's activity, the concentration of Fe on the surface of Fe-$TiO_2$ and C-Fe $TiO_2$ nanoparticles was measured by EDX analysis shown in Fig. 3.
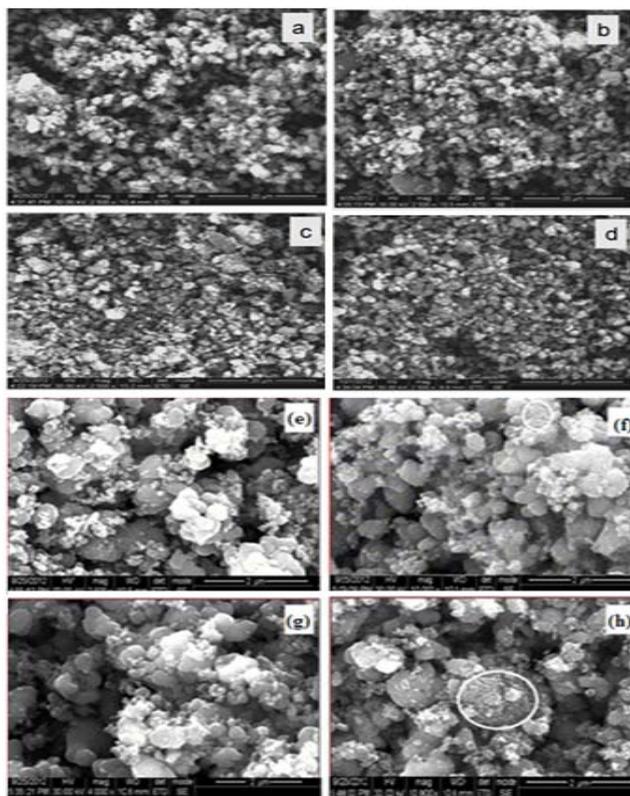
Fig. 2 SEM micrographs of (a) $Fe_{0.2}TiO_2NP$ (b) $Fe_{0.5}TiO_2NP$ (c) $Fe_{1.0}TiO_2NP$ (d) $Fe_{2.0}TiO_2NP$ (e) $C_{2.0}Fe_{1.0}TiO_2NP$ (f)$C_{2.0}Fe_{2.0}TiO_2NP$ (g) $C_{4.0}Fe_{1.0}TiO_2NP$ (h) $C_{4.0}Fe_{2.0}TiO_2NP$
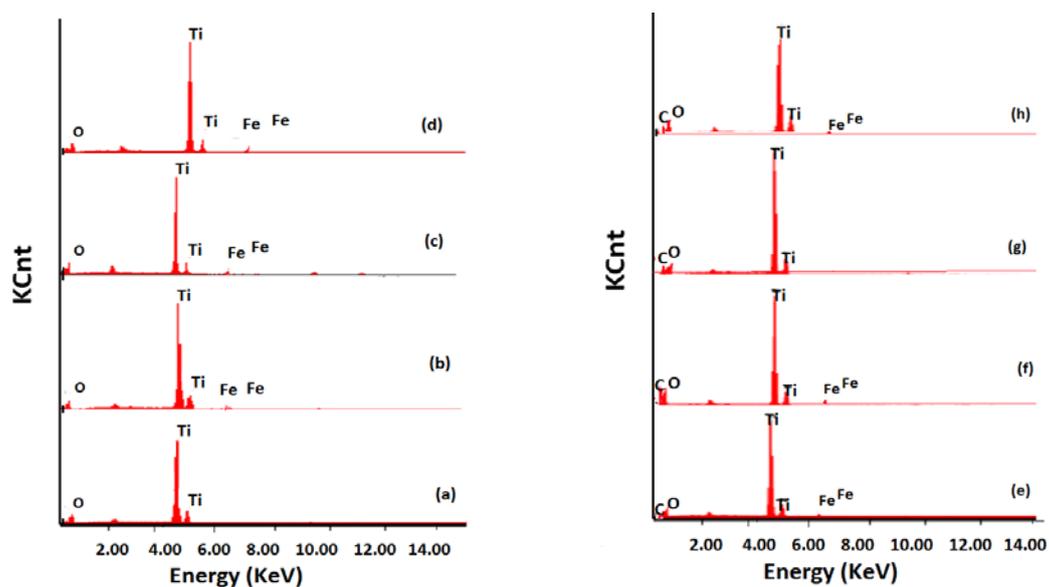


Fig. 3 EDX spectra of (a) $Fe_{0.2}TiO_2NP$ (b) $Fe_{0.5}TiO_2NP$ (c) $Fe_{1.0}TiO_2NP$ (d) $Fe_{2.0}TiO_2NP$ (e) $C_{2.0}Fe_{1.0}TiO_2NP$ (f)$C_{2.0}Fe_{2.0}TiO_2NP$ (g) $C_{4.0}Fe_{1.0}TiO_2NP$ (h) $C_{4.0}Fe_{2.0}TiO_2NP$

From EDX analysis, it was observed that the concentration of iron incorporated in Fe-TiO$_2$ and C-Fe TiO$_2$ catalysts was lower than the concentration of iron added during the preparation procedure. This is true for doped nanocatalysts prepared by sol-gel routes due to the reason that the doped ions are distributed un-uniformly within or on the surface of titania particles, making it difficult to control the dopant amount incorporated in the catalyst (Wong *et al.* 2004). During the preparation of Fe-TiO$_2$, the amount of iron added to the reaction mixture was 0.2 wt%, 0.5 wt%, 1.0 wt% and 2.0 wt% respectively for the catalyst Fe$_{0.2}$TiO$_2$NP, Fe$_{0.5}$TiO$_2$NP, Fe$_{1.0}$TiO$_2$NP and Fe$_{2.0}$TiO$_2$NP. From the EDX spectra of Fe-TiO$_2$ catalysts, the amount of Fe estimated in the catalysts was 0 wt%, 0.3 wt%, 0.7 wt% and 1.1 wt% respectively. During the preparation of C-Fe TiO$_2$ catalysts, the amount of iron added to the reaction mixture was 1.0 wt% for the catalyst C$_{2.0}$Fe$_{1.0}$TiO$_2$NP and C$_{4.0}$Fe$_{1.0}$TiO$_2$NP; and 2.0 wt% for the catalyst C$_{2.0}$Fe$_{2.0}$TiO$_2$NP and C$_{4.0}$Fe$_{2.0}$TiO$_2$NP. From EDX analysis, the amount of Fe estimated in the catalysts C$_{2.0}$Fe$_{1.0}$TiO$_2$NP, C$_{2.0}$Fe$_{2.0}$TiO$_2$NP, C$_{4.0}$Fe$_{1.0}$TiO$_2$NP and C$_{4.0}$Fe$_{2.0}$TiO$_2$NP was 0.6 wt%, 1.2 wt%, 0.32 wt% and 0.98 wt% respectively.

### 3.3.1 Visible light characterization

The UV-Vis absorption spectra of pure TiO$_2$, Fe-TiO$_2$ and C-Fe TiO$_2$ nanoparticles are illustrated in Fig. 4. The undoped titania sample was found to have absorption only in the UV region, whereas, all the Fe-TiO$_2$ catalysts possessed a slight red shift towards visible light region. The absorption edge of the higher iron loaded sample Fe$_{2.0}$TiO$_2$NP laid around 410 nm corresponding to a band gap of 3.02 eV (calculated using Eq. (3)).

$$E_g = 1239.8 / \lambda \tag{3}$$

All the codoped samples exhibit better UV-Vis absorption than the pristine or Fe-TiO$_2$ catalysts, and the catalyst 'C$_{2.0}$Fe$_{2.0}$TiO$_2$NP' was found to possess superior light absorption properties than the other samples. The onset of absorption in the catalyst took place at the
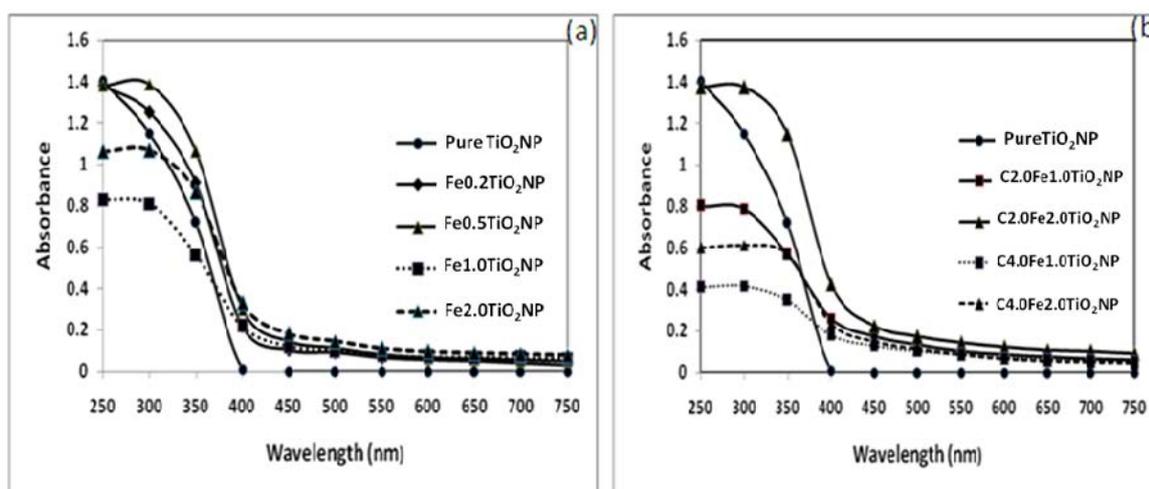


Fig. 4 UV-Vis Absorption Spectra of (a) pure and iron doped catalysts (b) pure and carbon-iron codoped catalysts

wavelength of 420 nm corresponding to a band gap of 2.95 eV. The red shift clearly shows the modification of $TiO_2$ crystal lattice with carbon and iron, rather than coating of the catalyst surface. This result is supported by the study conducted by Wu et al., in which a control experiment was carried out with a coating of carbon on the surface of P-25 titania film and the UV-Vis spectrum was obtained (Wu *et al.* 2007). The spectrum was similar to the pure P-25 titania film with no absorption in the visible region, hence it was reported that obvious absorption shift will be observed only when there is a change in catalyst crystal lattice.

### 3.4 Surface area analysis

BET specific surface area analysis was accomplished for each category of catalyst to identify the change in surface area after doping or co-doping. The specific surface area of pure $TiO_2$ was very large and found to be 180 $m^2/g$ and that of Fe-$TiO_2$ catalyst ($Fe_{2.0}TiO_2NP$) and C-Fe-$TiO_2$ catalyst ($C_{2.0}Fe_{2.0}TiO_2NP$) was 105 $m^2/g$ and 91$m^2/g$ respectively. This pattern of surface area reduction was also observed by Praveen Surolia et al., during the impregnation of ferric salts on pure $TiO_2$, in which the surface area of the pure catalyst was 50 $m^2/g$ and reduced to 43 $m^2/g$ and 15 $m^2/g$ after impregnation with ferric chloride and ferric sulphate (Praveen Surolia *et al.* 2007). The drop in surface area while doping with chloride and sulphate salts is reported to be due to chlorination and sulfation which takes place upon the crystalline oxide. The result is also supported by Liu *et al.*, who noticed that the surface area and pore volume of iron titanate catalyst decreased to a certain extent due to the formation of sulfate species (Liu *et al.* 2011).

However, it is to be noted that all the catalysts synthesized in this work possess a very larger surface area than the commercially renowned Degussa P25 catalyst which is 50 $m^2/g$ (Ahmed et al. 2010).

On the other hand, the sulfation process can greatly increase the strong acid sites in catalysts, which significantly promotes the performance of the catalyst. This justification is in accord with the study by Shujuan Zhang *et al.*, in which the sulfation process improved the dispersion of Ni species and provided strong Bronsted and Lewis acid sites, which contributed to a high catalytic activity for propane selective reduction of NO (Shujuan Zhang *et al.* 2005).

### 3.5 Coupled semiconductor photo-Fenton's decolorization of dyes by Fe-$TiO_2$ nanoparticles

In the semiconductor photo-Fenton's decolorization of dyes, a detailed investigation on the role of initial pH of the dye solution was carried out between pH 3.0 and pH 9.0. Studies were not conducted below pH 3.0 due to the fact that under strong acidic conditions, $TiO_2$ particles tend to agglomerate and the surface area available for dye adsorption and photon absorption would be reduced (Fox and Dulay 1993, Chen and Gu 2002, Yu *et al.* 2007, Akpan and Hameed 2009). Fig. 5 illustrates the semiconductor photo-Fenton's decolorization of BB and AO with pure and Fe-$TiO_2$ catalysts at varied pH.

It could be observed that the catalyst '$Fe_{2.0}TiO_2NP$' with higher amount of iron was found to decolourize both the dyes at a faster rate, which might be ascribed to the enhanced photo-Fenton's property at higher iron loading. The enhancement in the activity of Fe-$TiO_2$ catalysts over pure titania might be due to the coupling of Fenton's process and photocatalytic mechanism which synergistically destructed the dye pollutants.

On further observing the decolorization pattern, BB decolorization occurred at a rapid rate at
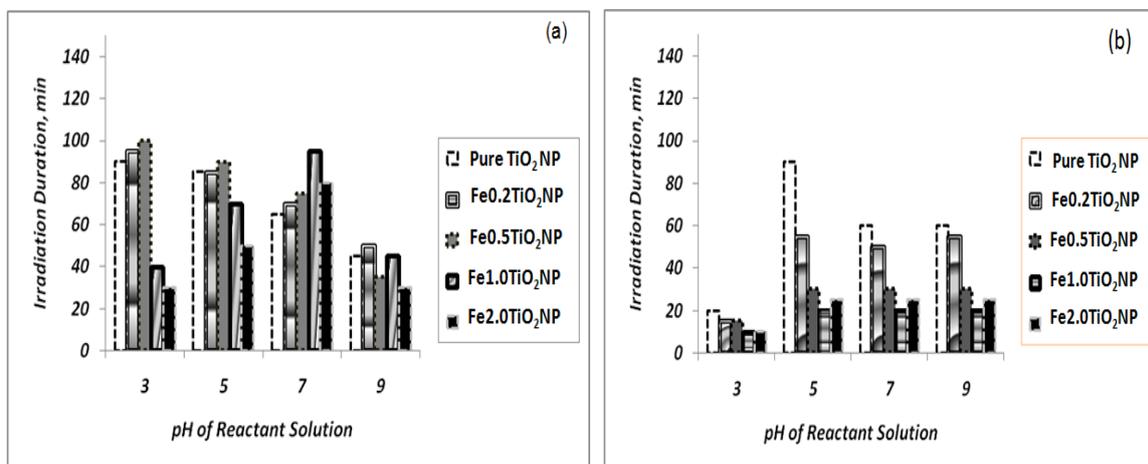
Fig. 5 Coupled semiconductor photo-Fenton's decolorization of (a) BB dye and (b) AO dye with pure and Fe-TiO$_2$ nanotitania at varied pH (Experimental conditions: Catalyst dosage=0.5 g/L; H$_2$O$_2$ concentration=29.7 mmol/L; Initial solar intensity during BB decolorization=~60kiloLUX; Initial solar intensity during AO decolorization=>90kiloLUX)
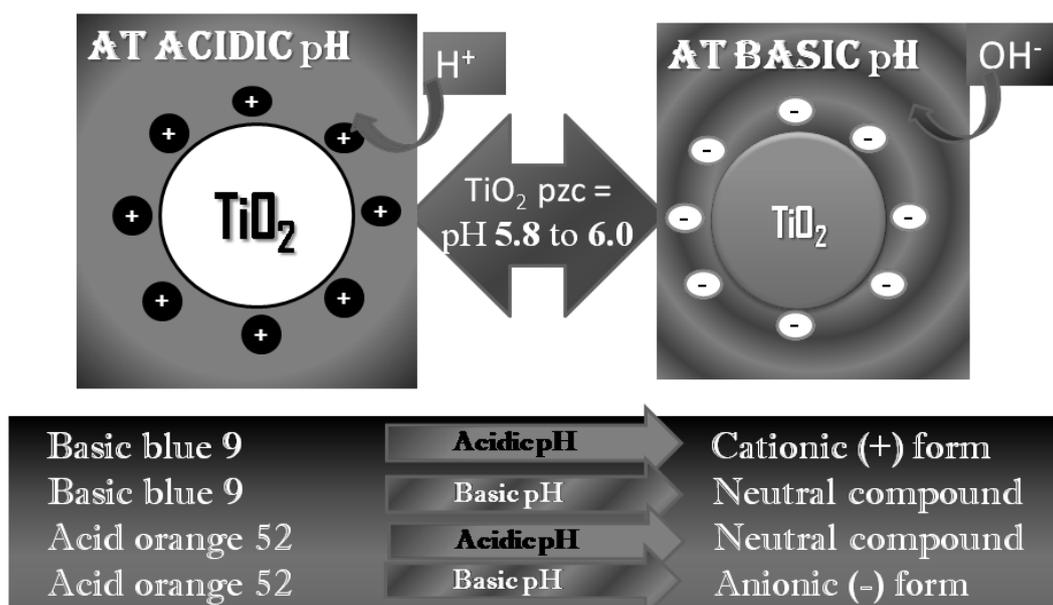


Fig. 6 Dye-Catalyst interaction at acidic pH and basic pH

pH 3.0 and 9.0, at which a complete decolorization was observed within 30 min of solar irradiation with Fe$_{2.0}$TiO$_2$NP, when compared to the decolorization at pH 5.0 and pH 7.0. The enhanced degradation in acidic pH was due to the well known Fenton's process which is generally efficient at pH around 3.0 (Ghaly *et al.* 2001, Zhang *et al.* 2005). The rapid degradation of BB at pH 9.0 might be due to the enhanced catalyst-cationic dye interaction at basic pH as shown in Fig. 5 to Fig. 6 and explained as follows: For TiO$_2$, the point of zero charge (pzc) is around 5.8 to 6.0.

Hence, at acidic pH below 5.8, the aqueous medium supplies more protons and make the particle surface possess large number of positive charge. Whereas, at pH above 5.8, the aqueous medium provides hydroxyl ions and the particle surface possesses negative charge. Since BB is a cationic dye, it is believed to be predominantly in its cationic form at acidic pH and neutral form at basic pH. Therefore at basic pH, the electrostatic repulsion between the negatively charged catalyst surface and the neutral dye molecule is lower than the strong repulsion between the positively charged catalyst surface and positively charged BB dye at acidic pH.

In the case of AO, the dye was found to undergo rapid degradation at pH 3.0 and followed downward trend on increasing the pH from pH 3.0 to pH 9.0 (Torrades and Garcia 2014). This may also be due to the pzc of catalyst and the dissociation nature of the dye as illustrated in Fig. 6.

### 3.6 Coupled semiconductor photo-Fenton's decolorization of dyes by C-Fe TiO$_2$ nanoparticles

The decolorization results of BB and AO with a series of C-Fe codoped titania nanoparticles are shown in Figs. 7(a) and 7(b) respectively. It could be observed from the decolorizaiton results that the efficiency of the catalysts increased with an increase in Fe concentration irrespective of the amount of carbon, and the catalyst 'C$_{2.0}$Fe$_{2.0}$TiO$_2$NP' was found to be the best performer than the other combinations. As observed with the Fe-TiO$_2$ catalysts, the decolorization of BB with C-Fe nanotitania was effective at pH 3.0 and pH 9.0; and the AO decolorization was well pronounced at pH 3.0. As explained in the earlier section, the enhanced decolorization of both the dyes at acidic pH was due to enhanced Fenton's activity around pH 3.0. In the case of BB, since the anchoring of S+ of the dye on to the catalyst surface is better at basic pH, the degradation was efficient at pH 9.0 as well. In the case of AO, since both the Fenton's activity and anchoring of $-SO_3^-$ of the dye on to the catalyst surface is favorable at pH 3.0, efficient degradation of AO was observed only at acidic pH. This is in accord with the results obtained by Zhiyong *et al*. (2007) in which the decolorization of azo dye orangeII was favoured at acidic pH 3.0 and found to be inefficient at basic pH 10.0 (Zhiyong *et al*. 2007).
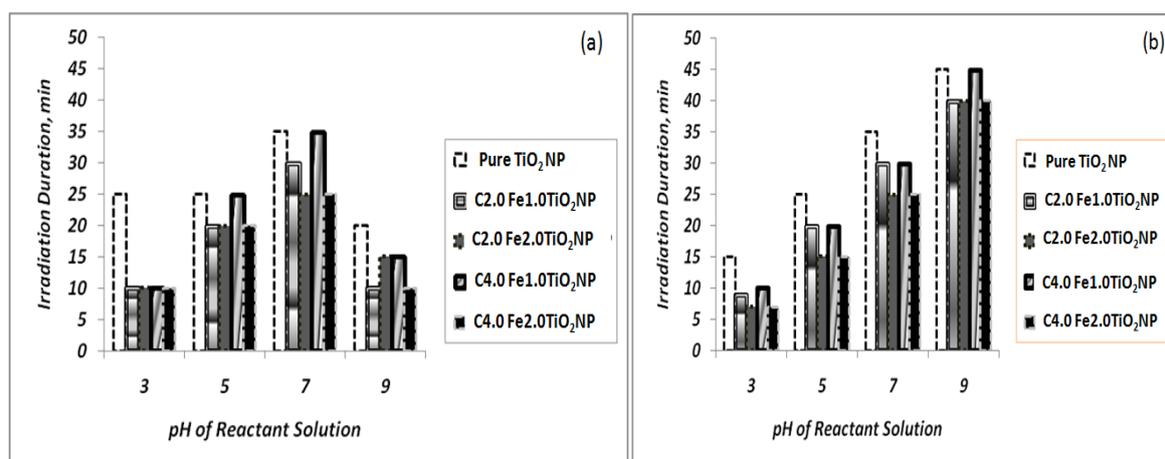


Fig. 7 Coupled semiconductor photo-Fenton's decolorization of (a) BB (b) AO with pure and C-Fe codoped nanotitania at varied pH (Initial solar intensity (BB) = ~55 kiloLUX; Initial solar intensity (AO)=~50 kiloLUX)

### 3.7 Selection of efficient catalyst

While observing the degradation of the dyes with the pristine, iron doped and carbon-iron codoped catalysts, the degradation was found to be very efficient with the catalysts, "$Fe_{2.0}TiO_2NP$, $C_{2.0}Fe_{2.0}TiO_2NP$ and $C_{4.0}Fe_{2.0}TiO_2NP$". It could be noted that in the previous sections, all the experiments were conducted with different catalysts at virtually similar experimental conditions except the solar intensity, which inevitably varied between 50,000 LUX and >80,000 LUX in majority of the photochemical studies. Hence, in order to select the best catalyst, experiments were repeated with the efficient catalysts keeping the initial dye concentration as 10 ppm, catalyst dosage as 0.5 g/L, $H_2O_2$ concentration as 29.7 mmol/L at pH 3 and all the dye suspensions were simultaneously subjected to solar irradiation under similar solar intensity (~60,000 LUX). The catalyst '$C_{2.0}Fe_{2.0}TiO_2NP$' was observed to be the most efficient among the other catalysts, which might be due to i) the suitable ratio of anatase and rutile phases ii) the largest amount of iron incorporation and iii) the enhanced visible light absorption characteristics. Hence further optimization studies were conducted with the catalyst '$C_{2.0}Fe_{2.0}TiO_2NP$'.

### 3.8 Effect of catalyst dosage

To study the effect of catalyst dosage in dye decolorization, four different dosages such as 0.25 g/L, 0.5 g/L, 0.75 g/L and 1.0 g/L (Akpan and Hameed 2009, Ahmed Hasaan Ali 2013) were studied and the results are shown in Figs. 8(a) and 8(b) for BB and AO respectively.

BB dye decolorization occurred at a faster rate when the amount of catalyst was increased from 0.25-0.75 g/L, which might be due to the enhanced Fenton's activity from larger number of active iron sites. The efficiency was leveled off with further increase in the catalyst load from 0.75 g/L to 1 g/L. In the case of AO, complete decolorization occurred at a faster rate when the amount of catalyst was increased from 0.25 to 1.0 g/L as shown in Fig. 7(b). Hence, further optimization studies in BB and AO decolorization were conducted with 0.75 g/L and 1 g/L of catalyst as optimum dosage respectively.
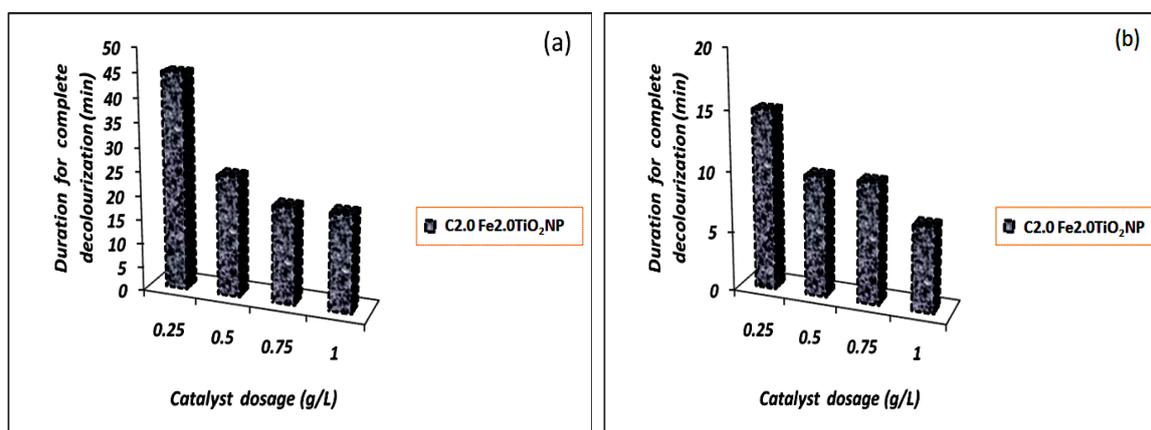


Fig. 8 Effect of catalyst dosage in the decolorization of (a) BB and (b) AO (Experimental conditions : Initial concentration of dye=10 ppm; $H_2O_2$ concentration=29.7 mmol/L; Initial solar intensity ~55,000 LUX)
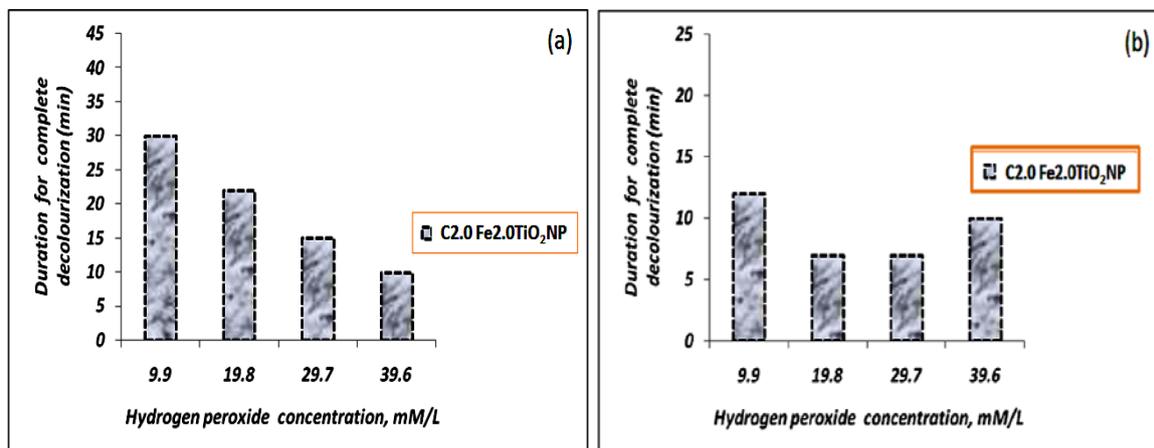
Fig 9. Effect of hydrogen peroxide concentration in the decolorization of (a) BB(b) AO dye (Experimental conditions : Initial concentration of dye = 10 ppm; Catalyst dosage = 0.75 g/L (for BB), 1.0 g/L (for AO); Initial solar intensity ~60,000 LUX)

### 3.9 Effect of $H_2O_2$ concentration

To study the effect of $H_2O_2$ concentration in dye decolorization, the concentration of $H_2O_2$ was varied as 9.9 mmol/L, 19.8 mmol/L, 29.7 mmol/L and 39.6 mmol/L, and the results are illustrated in Figs. 9(a) and 9(b) respectively.

Complete decolorization of BB dye was observed at a faster rate at higher $H_2O_2$ concentration of 39.6 mmol/L, which could be due to the fact that as the concentration of $H_2O_2$ increased, the concentration of hydroxyl radicals increased and led to enhanced oxidation. Hence, further degradation studies with BB were conducted with 39.6 mmol/L as optimum $H_2O_2$ concentration.

On the other hand, complete decolorization of AO was observed at a faster rate when the concentration of $H_2O_2$ was 19.8 mmol/L. The rate of decolorization remained constant when the oxidant concentration was increased from 19.8 mmol/L to 29.7 mmol/L and decreased when the concentration was further increased to 39.6 mmol/L. This could be explained in such a manner that the concentration of hydroxyl radicals increased with increase in $H_2O_2$ concentration from 19.8 mmol/L to 29.7 mmol/L, leading to increased rate of decolorization. The retarded rate at higher oxidant concentration might be due to the fact that at very higher $H_2O_2$ concentrations, $H_2O_2$ itself can act as a scavenger of hydroxyl radicals and render them unavailable for Fenton's reaction (Tamimi *et al*. 2008, Karthikeyan *et al*. 2011). Hence, the optimum $H_2O_2$ concentration was taken as 19.8 mmol/L in the case of AO dye.

### 3.10 Effect of initial pollutant concentration and kinetics

To examine the effect of initial dye concentration, the experiments were conducted at optimum conditions of pH, catalyst dose and $H_2O_2$ concentration, varying only the initial concentration of dye from 20 ppm to 50 ppm and the results are furnished in Table 1.

For both BB and AO, complete decolorization was achieved for the entire concentration range studied from 20 ppm to 50 ppm. On observing the degradation and mineralization pattern from Table 1, the amount of COD and TOC removal of BB was found to increase with increase in the

Table 1 Effect of Initial dye concentration in the degradation and Mineralization of dyes [Experimental conditions: catalyst dosage=0.75 g/L (BB), 1.0 g/L (AO); Initial pH of dye solution=pH 3; $H_2O_2$ concentration=39.6 mmol/L (BB), 19.8 mmol/L (AO); Initial Solar Intensity ~30 kiloLUX (BB), ~70 kiloLUX (AO)]

| SI. No. | Initial conc., of dye (ppm) | COD removal for BB dye (%) | TOC removal for BB dye (%) | COD removal for AO dye (%) | TOC removal for AO dye (%) |
|---|---|---|---|---|---|
| 1. | 20 | 91.3 | 88 | 91.3 | 90.3 |
| 2. | 30 | 88 | 83 | 86.7 | 87.3 |
| 3. | 40 | 80.9 | 78 | 67.1 | 58 |
| 4. | 50 | 77.9 | 70.1 | 49.1 | 36 |

Table 2 Optimum $COD:H_2O_2$ ratio for the semiconductor photo-Fenton's degradation of acid orange 52

| SI. No. | AO dye concentration, mg/L | COD, mg/L | $H_2O_2$ consumed, mg/L | $COD:H_2O_2$ ratio | Average $COD:H_2O_2$ ratio |
|---|---|---|---|---|---|
| 1. | 30 | 64 | 673 (19.8 mmol/L) | 1:10.5 | 1:10 |
| 2. | 50 | 98 | 945 (29.7 mmol/L) | 1:9.6 | |

initial dye concentration. In the case of AO, the amount of COD and TOC removal was found to increase when the initial concentration was increased till 30 ppm and decreased with further increase in concentration above 30 ppm. This may be due to the reason that the given $H_2O_2$ concentration of 19.8 mmol/L was sufficient for effective degradation up to 30 ppm and became insufficient with further increase in dye concentration. Hence the $H_2O_2$ concentration was increased from 19.8 mmol/L to 29.7 mmol/L to degrade 50 ppm of AO dye, and it was found that effective degradation (>94%) of the highest dye concentration was possible at the $H_2O_2$ concentration of 29.7 mmol/L.

In order to calculate the optimum $COD:H_2O_2$ ratio for AO degradation (for application in real textile effluent treatment), the COD value for 30 ppm and 50 ppm of AO dye and the amount of $H_2O_2$ consumed for the respective dye concentration was taken into account as given in Table 2.

From the table, the optimum $COD:H_2O_2$ for the coupled semiconductor photo-Fenton's degradation of 30 ppm and 50 ppm of AO was found to be 1:10. In order to study the kinetics of dye degradation, first and second order kinetic equations (Eqs. (4) and (5)) were applied, and the reaction kinetics were found to fit the first order rate equation with a regression co-efficient of 0.9 for both the dyes, and unfits the second order kinetics with a regression co-efficient of 0.5 for BB and 0.7 for AO respectively. Though the hydroxyl radical attack and Fenton's activity also played major roles in the degradation process, the kinetics clearly reveals that those factors only have a pseudo effect. Hence, it could be stated that the reaction followed a pseudo first order kinetics

$$k_1 = \frac{1}{t} \ln \frac{CP_0}{CP_t} \tag{4}$$

$$k_2 = \frac{1}{t} \left( \frac{CP_0}{CP_0 * CP_t} \right)$$

(5)

Where,

$k_1$=First order rate constant, min$^{-1}$

$k_2$=Second order rate constant, L/mg.min$^{-1}$

t=time, min

$CP_0$=Concentration of pollutant at t=0, mg/L

$CP_t$=Concentration of pollutant at any time "t", mg/L

The pseudo first order rate constants for the TOC removal of 10 ppm to 50 ppm of BB dye was found to be 0.115 min$^{-1}$, 0.066 min$^{-1}$, 0.043 min$^{-1}$, 0.032 min$^{-1}$ and 0.022 min$^{-1}$ respectively. The corresponding half lives ($t_{1/2}$) were 6.0 min, 10.5 min, 16.1 min, 21.6 min and 31.5 min respectively. The pseudo first order rate constants for the TOC removal of 10 ppm to 30 ppm of AO dye at optimized conditions with 19.8 mmol/L $H_2O_2$ was found to be 0.40 min$^{-1}$, 0.21 min$^{-1}$ and 0.154 min$^{-1}$ respectively. The corresponding half lives ($t_{1/2}$) were 1.7 min, 3.2 min and 4.5 min respectively. The pseudo first order rate constant and half life for the TOC removal of 50 ppm of AO dye with 29.7 mmol/L of $H_2O_2$ were 0.109 min$^{-1}$ and 6.4 min respectively.

Table 3 Characterization of textile dye bath effluent

| SI. No. | Parameter | Amount in dye bath effluent (Average of two values) |
|---------|-----------|-----------------------------------------------------|
| 1. | Color at 628 nm (Absorbance units) | 0.73 |
| 2. | pH | 10.1 |
| 3. | EC (mS/cm) | 49 |
| 4. | TDS (mg/L) | 37,640 |
| 5. | $Na^+$ (mg/L) | 5,782 |
| 6. | $Cl^-$ (mg/L) | 8,799 |
| 7. | Total Hardness as $CaCO_3$ (mg/L) | 467 |
| 8. | Calcium as $CaCO_3$ (mg/L) | 167 |
| 9. | $Mg^{2+}$ (mg/L) | 73 |
| 10. | Phenolphthalein alkalinity as $CaCO_3$ (mg/L) | 1,996 |
| 11. | Total alkalinity as $CaCO_3$ (mg/L) | 8,695 |
| 12. | $CO_3^{2-}$ (mg/L) | 3,995 |
| 13. | $HCO_3^-$ (mg/L) | 4,700 |
| 14. | $SO_4^{2-}$ (mg/L) | 2,043 |
| 15. | COD (mg/L) | 302 |
| 16. | TOC (mg/L) | 84 |

Table 4 Decolorization, degradation and mineralization of textile dye bath effluent [Experimental conditions: Initial pH of reactant solution=pH 3; Catalyst dosage=4 g/L; COD:$H_2O_2$ ratio=1:10; Initial solar intensity=35-40 kiloLUX]

| SI. No. | Irradiation Duration (min) | Color removal (%) | COD removal (%) | TOC removal (%) |
|---------|---------------------------|-------------------|-----------------|-----------------|
| 1. | 60 | 68 | 49.3 | 18.1 |
| 2. | 120 | 100 | 61.8 | 36.3 |
| 3. | 180 | - | 69.7 | 62.5 |
| 4. | 240 | - | 93.4 | 77.7 |

### *3.11 Application in real textile effluent treatment*

The practical application potential of the efficient catalyst, "$C_{2.0}Fe_{2.0}TiO_2NP$" was evaluated for the treatment of real textile effluent (exhausted dye bath effluent). As the dyes present in the collected wastewater have the properties similar to acid orange 52, the experimental conditions optimized in the degradation of acid orange 52 were applied for the treatment of the textile effluent.

The characteristics of the exhausted dye bath effluent are furnished in Table 3.

From the table, it could be noted that the COD of the dye bath effluent was low, but, similar low COD values have also been reported in the dye bath effluents of many other small scale textile industries (Ranganathan *et al*. 2007). The collected wastewater was screened to remove floatable solids, sand filtered to remove suspended solids and subjected to semiconductor coupled photo-Fenton's treatment. The COD and TOC of the sand filtered effluent were 294 mg/L and 76 mg/L respectively.

The experimental results are furnished in Table 4, where it could be observed that a complete color removal was achieved within 120 min of solar irradiation. Rate of COD removal was high in the initial period and it was gradual as the concentration of pollutants decreased. In spite of the hyper- salinity in the dye bath effluent, 93.4% of COD removal and 77.7% of TOC removal was achieved under the influence of very low solar intensity (35-40 kiloLUX). This reveals the practical applicability of this process for the potential treatment of real wastewater.

## 4. Conclusions

In summary, pristine $TiO_2$ nanoparticles were prepared and subjected to iron doping and carbon-iron codoping employing natural and eco-benign precursors, and energy efficient methods. Among the synthesized catalysts, the codoped catalyst, '$C_{2.0}Fe_{2.0}TiO_2NP$' was found to contain suitable fraction of 66% of anatase and 34% of rutile phases respectively. $C_{2.0}Fe_{2.0}TiO_2NP$ was found to possess enhanced visible light absorption properties and efficient degradation properties in the solar photochemical experiments which is attributed to the beneficial adsorption of pollutants on to carbon and enhanced Fenton's activity from higher iron loading. The degradation of the dyes, basic blue 9 and acid orange 52 was efficient at the pH at which the Fenton's activity and catalyst-dye interaction was high. The semiconductor coupled solar photo-Fenton's

degradation of the dyes followed pseudo first order kinetics. In textile dye bath treatment, complete color removal, effective COD removal and TOC removal was achieved under very low solar intensity of 35-40 kiloLUX. Overall, the current study reveals that the natural solar energy is a viable alternative to the energy intensive treatment technologies for eradicating dye pollutants.

## Acknowledgements

## References

Ahmed, S., Rasul, M.G., Martens, W.N., Brown, R.J. and Hashib, M.A. (2010), "Heterogeneous photocatalytic degradation of phenols in wasterwater: a review on current status and developments", *Desalination*, **261**(1-2), 3-18.

Ahmed Hassan Ali (2013), "Study on the photocatalytic degradation of indigo carmine dye by $TiO_2$ photocatalyst", *J. Kerbala Univ.*, **11**(2), 145-153.

Akpan, U.G. and Hameed, B.H. (2009), "Parameters affecting the photocatalytic degradation of dyes using $TiO_2$ based photocatalysts: A review", *J. Haz. Mater.*, **170**(2), 520-529.

Avisar, D., Horovitz, I., Lozzi, L., Ruggieri, F., Baker, M., Abel, M. L., Ghaly, M.Y., Georg, H., Roland, M. and Roland, H. (2001), "Photochemical oxidation of p-chlorophenol by $UV/H_2O_2$ and photo-Fenton process. A comparative study", *Waste Manage.*, **21**(1), 41-47.

APHA (2005), *Standard methods for the examination of water and wastewater*, American Public Health Association, Washington, DC.

Chen, X. and Gu, G. (2002), "Study on synthesis of nanometer $TiO_2$ crystal from organic compound in liquid phase at normal pressure and low temperature", *Chin. J. Inorg. Chem.*, **18**(7), 749-752.

Fox, M.A. and Dulay, M.T. (1993), "Heterogeneous photocatalysis", *Chem. Rev.*, **93**(1), 341-350.

Ghaly, M.Y., Georg, H., Roland, M. and Roland, H. (2001), "Photochemical oxidation of p-chlorophenol by $UV/H_2O_2$ and photo-Fenton process - A comparative study", *Waste Manage.*, **21**(1), 41-47.

Hamadanian, M., Reisi-Vanani, A., Behpour, M. and Esmaeily, A.S. (2011), "Synthesis and characterization of Fe, S-codoped $TiO_2$ nanoparticles: Application in degradation of organic water pollutants", *Desalination*, **281**, 319-324.

Hussain, S.T. and Siddiqa, A. (2011), "Iron and chromium doped titanium dioxide nanotubes for the degradation of environmental and industrial pollutants", *Int. J. Environ. Sci. Tech.*, **8**(2), 351-362.

Jeevitha Raji, R. and Palanivelu, K. (2011), "Sunlight-induced photocatalytic degradation of organic pollutants by carbon-modified nanotitania with vegetable oil as precursor", *Ind. Eng. Chem. Res.*, **50**(6), 3130-3138.

Jeevitha Raji, R., J., Min-Jung, Im, Ji-Sun, Lee, Y.S. and Palanivelu, K. (2013), "Electrospinning of polymer unaided $TiO_2$ fibers and iron impregnation for sunlight-induced photo-Fenton's degradation of dyes", *Environ. Eng. Sci.*, **30**(11), 653-662.

Jongsomjit, B., Tipnapa, W. and Piyasan, P. (2005), "Study of cobalt dispersion on titania consisting various rutile:anatase ratios", *Mater. Chem. Phys.*, **92**(2), 572-279.

Kamat, P.V. and Dan, M. (2002), "Nanoparticles in advanced oxidation processes", *Curr. Opin. Colloid Interf. Sci.*, **7**(5), 282-287.

Karthikeyan, S., Titus, A., Gnanamani, G., Mandal, A.B. and Sekaran, G. (2011), "Treatment of textile wastewater by homogeneous and heterogeneous Fenton oxidation processes", *Desalination*, **281**, 438-445.

Kavitha, P., Shavonda, M., Changseok, H., Miguel, P., Xiaojia, H., Dionysios, D. and Huey, H. (2013),

"Photoinactivation of Escherichia coli by sulfur-doped and nitrogen-fluorine-codoped $TiO_2$ nanoparticles under solar simulated light and visible light irradiation", *Environ. Sci. Technol.*, **47**(17), 9988-9996.

Konecoglu, G., Toygun, S., Kalpakli, Y. and Akgun, M. (2015), "Photocatalytic degradation of textile dye CI Basic Yellow 28 wastewater by Degussa P25 based $TiO_2$", *Adv. Environ. Res.*, **4**(1), 25-38.

Korosi, L., Oszko. A., Galbacs, G., Richardt, A., Zollmer, V. and Dekany, I. (2007), "Structural properties and photocatalytic behaviour of phosphate-modified nanocrystalline titania films", *Appl. Catal. B: Environ.*, **77**(1), 175-181.

Li, C., Zhaohua, J. and Zhongping, Y. (2010), "Fabrication and characterization of multi-metal codopedtitania films for a water-splitting reaction", *Dalton Trans.*, **39**(44), 10692-10696.

Liu, F., Asakura, K., He, H. and Zang, C. (2011), "Influence of sulfation on iron titanate catalyst for the selective catalytic reduction of NOx with NH3", *Appl. Catal. B: Environ.*, **103**(3-4), 369-377.

Lucas, M.S. and Peres, J.A. (2006), "Decolorization of the azo dye Reactive Black 5 by Fenton and photo-Fenton oxidation", *Dyes Pigments.*, **71**(3), 236-244.

McEvoy, J.G., Wenquan, C. and Zisheng, Z. (2013), "Degradative and disinfective properties of carbon-doped anatase-rutile $TiO_2$ mixtures under visible light irradiation", *Catal. Today*, **207**, 191-199.

Murray, C.B., Kagan, C.R. and Bawendi, M.G. (2000), "Synthesis and characterization of Monodisperse nano crystals and close-packed nanocrystal assemblies", *Ann. Rev. Mater. Sci.*, **30**(1), 545-550.

Navalon, S., Alvaro, M. and Gracia, H. (2010), "Heterogeneous Fenton catalysts based on clays, silicas and zeolites", *Appl. Catal. B: Environ.*, **99**(1), 1-26.

Oliveria, L.C.A., Goncalves, M., Guerreiro, M.C., Ramalho, T.C., Fabris, J.D., Pereira, M.C. and Sapag, K. (2007), "A new catalyst material based on Niobia/Iron oxide composite on the oxidation of organic contaminants in water via heterogeneous Fenton mechanisms", *Appl. Catal. A: General*, **316**(1), 117-124.

Praveen Surolia, K., Rajesh Tayade, J. and Rakesh Jasra, V. (2007), "Effect of anions on the photocatalytic activity of Fe(III) salts impregnated $TiO_2$", *Ind. Eng. Chem. Res.*, **46**(19), 6196-6203.

Ranganathan, K., Karunagaran, K. and Sharma, D.C. (2007), "Recycling of wastewaters of textile dyeing industries using advanced treatment technology and cost analysis-Case studies", *Resour. Conserv. Recy.*, **50**(3), 306-318.

Shujuan, Zhang, Landong, Li, Fuxiang, Zhang and Naijia, Guan (2005), "Influence of sulfation on the catalytic activity of Ni-ZrO2 for NO reduction with propane in excess oxygen", *J. Nat. Gas Chem.*, **14**(4), 221-225.

Tamimi, M., Qourzal, S., Barka, N., Assambane, A. and Ait-Ichou, Y. (2008), "Methomyl degradation in aqueous solutions by Fenton'reagent and the photo-Fenton system", *Sep. Purif. Technol.*, **61**(1), 103-108.

Torrades, F. and García-Montaño, J. (2014), "Using central composite experimental design to optimize the degradation of real dye wastewater by Fenton and photo-Fenton reactions", *Dyes Pigments*, **100**, 184-190.

Wong, S.K., Jiyun, F., Xijun, H. and Po Lock, Y. (2004), "Discoloration and mineralization of non-biodegradable azo dye orange ii by copper-doped $TiO_2$ nanocatalysts", *J. Environ. Sci. Hlth., Part A*, **39**(10), 2583-2595.

Wu, G., Nishikawa, T., Ohtani, B. and Chen, A. (2007), "Synthesis and characterization of carbon doped $TiO_2$ nanostructures with enhanced visible light response", *Chem. Mater.*, **19**(18), 4530-4537.

Yu, H., Zheng, X., Yin, Z., Tao, F., Fang, B. and Hou, K. (2007), "Preparation of nitrogen-doped $TiO_2$ nanoparticle catalyst and its catalytic activity under visible light", *Chin. J. Chem. Eng.*, **15**(6), 802-807.

Zhang, H., Heung, J.C. and Chin-Pao, H. (2005), "Optimization of Fenton process for the treatment of landfill leachate", *J. Haz. Mater.*, **125**(1-3), 166-174.

Zhao, B., Giuseppe, M., Iolanda, P., Jun, L., Leonardo, P. and Giuseppe, V. (2010), "Degradation of 4-nitrophenol (4-NP) using Fe-$TiO_2$ as a heterogeneous photo-Fenton catalyst", *J. Haz. Mater.*, **176**(1), 569-574.

Zhiyong, Y., Bensimon, M. and Sarria, V. (2007), "$ZnSO_4$ $TiO_2$ catalyst with higher photocatalytic activity", *Appl. Catal. B: Environ.*, **76**(1), 185-195.

*WL*